

铁镍磷化物催化剂在 CO 加氢制低碳醇反应中的应用

宋宪根^{1,3}, 丁云杰^{1,2,*}, 陈维苗¹, 董文达^{1,3}, 裴彦鹏^{1,3}, 臧娟^{1,3}, 严丽¹, 吕元¹

¹中国科学院大连化学物理研究所清洁能源国家实验室, 辽宁大连 116023

²中国科学院大连化学物理研究所催化基础国家重点实验室, 辽宁大连 116023

³中国科学院研究生院, 北京 100049

摘要: 通过程序升温还原法制备了一系列氧化硅负载的不同 P/M (M = Fe 和 Ni) 摩尔比的金属磷化物催化剂, 在 553 K, 5.0 MPa 和 H₂:CO = 2 (摩尔比) 的反应条件下用固定床反应器测试了它们催化 CO 加氢反应性能。结果表明, 在 FeP_x/SiO₂ (x 为 P/M 摩尔比) 催化剂上, 液相产物是以甲醇为主的低碳含氧化物的混合物。而在 NiP_x/SiO₂ 催化剂上, 气态产物主要为甲烷, 液相产物绝大多数是甲醇。表征结果表明, 磷化物催化剂上的 Fe₂P, Fe₃P, Ni, Ni₂P, Ni₃P 和 Ni₁₂P₅ 晶相在反应条件下是稳定的, 没有形成磷化物的金属铁, 在反应后转变成碳化铁晶相。

关键词: 一氧化碳; 加氢; 含氧化物; 金属磷化物; 磷化铁; 磷化镍; 氧化硅

中图分类号: O643 文献标识码: A

收稿日期: 2012-09-10. 接受日期: 2012-10-08.

*通讯联系人. 电话/传真: (0411)84379143; 电子信箱: dyj@dicp.ac.cn

基金来源: 国家自然科学基金 (20903090).

本文的英文电子版(国际版)由 Elsevier 出版社在 ScienceDirect 上出版 (<http://www.sciencedirect.com/science/journal/18722067>).

Synthesis of Mixed Alcohols from CO Hydrogenation over Iron and Nickel Metal Phosphide Catalysts

SONG Xiangen^{1,3}, DING Yunjie^{1,2,*}, CHEN Weimiao¹, DONG Wenda^{1,3}, PEI Yanpeng^{1,3}, ZANG Juan^{1,3}, YAN Li¹, LÜ Yuan¹

¹Dalian National Laboratory for Clean Energy, Dalian Institute of Chemical Physics, Chinese Academy of Science, Dalian 116023, Liaoning, China

²State Key Laboratory of Catalysis, Dalian Institute of Chemical Physics, Chinese Academy of Sciences, Dalian 116023, Liaoning, China

³Graduate University of Chinese Academy of Sciences, Beijing 100049, China

Abstract: A series of silica supported iron and nickel metal phosphides with different molar ratios of P to metal were synthesized by the temperature programmed reduction method. Their catalytic performance for CO hydrogenation in a fixed bed reactor was tested with the conditions of 553 K, 5.0 MPa, and H₂:CO = 2 (molar ratio). With the FeP_x/SiO₂ catalysts (x denotes the molar ratio of P to metal), the product was a mixture of oxygenates containing methanol as the major component. With the NiP_x/SiO₂ samples, the liquid product was mainly methanol. The Fe₂P, Fe₃P, Ni, Ni₂P, Ni₃P, and Ni₁₂P₅ phases were stable during CO hydrogenation, while most of the metallic Fe phase transformed into iron carbide.

Key words: carbon monoxide hydrogenation; oxygenates; metal phosphides; silica; iron phosphide; nickel phosphide

Received 10 September 2012. Accepted 8 October 2012.

*Corresponding author. Tel/Fax: +86-411-84379143; E-mail: dyj@dicp.ac.cn

This work was supported by the National Natural Science Foundation of China (20903090).

English edition available online at Elsevier ScienceDirect (<http://www.sciencedirect.com/science/journal/18722067>).

Concerns about diminishing non-renewable petroleum resources, global climate change, and the energy crisis have

increased interest in alternative fuel development, especially in biomass conversion. Biomass can be converted into

bio-ethanol by an enzymatic process [1]. At present, ethanol is produced on the large scale primarily via the fermentation of sugars derived from corn or sugar cane, or via the hydration of petroleum-based ethylene. The ethylene hydration route suffers from the problem of rising crude oil prices and dependence on oil imports. The production of fuel-grade ethanol from fermentation is unattractive because of energy intensive distillation steps. Therefore, a more flexible approach using biomass and coal gas gasification to syngas (CO, CO₂, and H₂) followed by the catalytic conversion of the syngas to ethanol and other oxygenated products can be the route to solve the crisis in the near future [1].

Many catalysts reported for the conversion of syngas to oxygenated hydrocarbon products, such as Rh-based catalysts [2–4], alkali-doped Cu-based catalysts [5,6], modified Fischer-Tropsch (FT) synthesis catalysts [7–9], and Mo-based catalysts [10–12], are limited by poor selectivity. Rh-based catalysts have the highest ethanol selectivity among the catalysts investigated [2–4]. However, the issues of cost and supply mean that it would be difficult to commercialize for large scale processes. Therefore, there is significant interest in developing alternative catalysts for selective ethanol synthesis from syngas.

Recently, transition metal phosphides [13–18] were tested in a series of hydrogenation reactions. Supported phosphides can be easily prepared by the temperature-programmed reduction of phosphate precursors. Some researchers [13–18] have suggested that the phosphide catalysts possessed catalytic properties similar to precious metals, and they can also resist sulphur poisoning. The ligand effect and ensemble effect after the insertion of P atoms into the lattice of the metal can change the electronic properties and adsorption properties of the metal [13,14]. These characteristics could endowed the phosphides with the properties for a potential application in syngas conversion. Zaman et al. [19–21] reported syngas conversion over MoP/SiO₂ catalysts and showed that this type of catalyst gave reduced selectivities to hydrocarbons and increased selectivities to oxygenated products. Based on the catalytic results from Mo phosphides [19–21] for syngas conversion and iron group metal phosphides for hydrogenation, we have studied the catalytic properties of iron and nickel metal phosphides for syngas conversion. FeP_x/SiO₂ and NiP_x/SiO₂ catalysts with different molar ratios of P to metal were prepared and characterized using temperature-programmed reduction (TPR), X-ray diffraction (XRD), CO temperature-programmed desorption (CO-TPD), and chemisorption techniques.

1 Experimental

1.1 Preparation of catalysts

The catalysts with different molar ratios of P to metal were prepared by a TPR method from supported phosphate precursors prepared by the incipient impregnation of the silica support. The silica support was calcined at 773 K for 3 h prior to use. To avoid the formation of an insoluble precipitate of the metal phosphate on mixing the aqueous solutions of metal nitrate and ammonium phosphate, a two-step impregnation was used to prepare the supported metal phosphate precursors. First, the silica support was impregnated with an aqueous solution of (NH₄)₂HPO₄. After drying at 393 K for 8 h, the support containing phosphorus was impregnated with the solution of metal nitrate. The impregnated supports were then dried at 393 K for 8 h and calcined at 773 K for 4 h. Second, the precursors were reduced to phosphides by heating from room temperature to 623 K at a ramping rate of 5 K/min and from 623 to 973 K at a ramping rate of 1 K/min. The samples were held at 973 K for 2 h in flowing H₂ with a flow rate of 350 ml/min per gram of precursor. The catalysts were cooled to room temperature in a H₂ flow and then passivated in a 1% O₂/Ar flow with a flow rate of 100 ml/min for 4 h. The catalysts with different molar ratios of P to metal were denoted as MP_x/SiO₂ ($x = P/M$ molar ratio). The metal mass loading of all catalysts was 10% while the P loading varied.

1.2 Characterization of the catalysts

TPR experiments were performed on a Micromeritics Autochem 2910 apparatus. The metal phosphate precursor (80 mg) was calcined at 773 K for 4 h and then placed in a quartz reactor and reduced by a 10% H₂/Ar gas mixture at a flow rate of 50 ml/min. The temperature increased at 10 K/min to the final temperature and hydrogen consumption was recorded by a thermal conductivity detector (TCD). A mass spectrometer (QMS, Balzers OmniStar 300) was used to monitor desorbed species. MS signals at $m/z = 2$ (H₂), 18 (H₂O), and 34 (PH₃) were continuously recorded.

The CO uptake was measured using the same apparatus as used for H₂-TPR. The sample (100 mg) was loaded into the reactor and reduced in a H₂ flow with a flow rate of 60 ml/min at 773 K for 2 h. Then, the sample was flushed at 773 K with He at a flow rate of 80 ml/min for 2 h. Subsequently, the sample was cooled to 323 K. The gas (5% CO-He) was injected into a He carrier gas with a flow rate of 50 ml/min. CO uptake was measured using a TCD. CO pulses were repeatedly injected until the areas of consecutive effluent pulses were constant. The total CO uptake was then calculated. After CO adsorption, the sample was swept with a He flow (20 ml/min) until the TCD signal was stable. CO-TPD was performed in the He flow (20 ml/min) at a heating rate of 10 K/min with a quadrupole mass spectrometer (QMS, Balzers OmniStar 300) as detector to

monitor the desorbed species. MS signals at $m/z = 2$ (H_2), 16 (CH_4), 18 (H_2O), 28 (CO), 44 (CO_2), and 12 (C) were continuously recorded.

The Brunauer-Emmett-Teller (BET) method was used to calculate the specific surface area. Pore size distributions were determined from the desorption branch of the isotherms using the Barrett-Joyner-Halenda (BJH) method. Powder X-ray diffraction (XRD) measurements were recorded with a PANalytical X'Pert-Pro powder X-ray diffractometer using $\text{Cu K}\alpha$ radiation ($\lambda = 0.15418 \text{ nm}$), operated at 40 kV and 150 mA. Both the fresh and spent catalysts used in the XRD measurements were first passivated.

1.3 Activity studies

The catalyst was pre-treated in the fixed bed reactor as described in the TPR section. After cooling to 553 K in H_2 flow, the gas was switched to syngas ($\text{H}_2:\text{CO} = 2$) and the reaction was carried out at 553 K, 5.0 MPa, and GHSV = 5000 h^{-1} . Supported pure metal catalysts of iron and nickel were also tested for comparison. The volume of catalyst loaded was 1 ml. The reaction system consisted of a small fixed bed tubular reactor made of 316 L stainless steel with 300 mm length and 9.0 mm inner diameter with an external heating system. The catalyst particles (20–40 mesh) were placed on a packed bed of quartz sand inside the reactor and the space above the catalyst was also filled with quartz sand that acted as a pre-heater for the syngas. The effluent was passed through a condenser filled with cold and de-ionized water (283 K) to collect the liquid products. The outlet gases CO , H_2 , CH_4 , CO_2 , and other $\text{C}_1\text{--C}_5$ hydrocarbons were analyzed online by an Agilent 3000A Micro GC with four packed columns (molecule sieve, PLOT Q, Al_2O_3 , and OV-1) and TCD detectors. The liquid organic products and the aqueous products were analyzed offline on a Varian 3800 GC with an HP-FFAP capillary column and a FID detector after they were carefully separated. CO conversion and product selectivity were calculated by the equations of conversion = $(\sum(n_i \times M_i)/M_{\text{CO}}) \times 100\%$ and selectivity = $(n_i \times M_i / \sum(n_i \times M_i)) \times 100\%$, where n_i is the number of carbon atoms in product i , M_i is the total mole number of product i , and M_{CO} is the total mole number of carbon monoxide in the feed.

2 Results and discussion

2.1 H_2 -TPR results

To study the interaction between the metal component and phosphorus, H_2 -TPR was carried out from room temperature to 1100 K. The H_2 -TPR profiles of the catalyst precursors are shown in Fig. 1. The catalyst precursors of

the $\text{FeP}_x/\text{SiO}_2$ samples after calcination were mixtures of iron oxide and iron phosphate, so, the TPR curves of the sample were the overlapped result of iron oxide and iron phosphate. Three reduction stages for silica supported iron oxide that corresponded to (1) Fe_2O_3 to Fe_3O_4 at 650 K, (2) Fe_3O_4 to FeO at 750 K, and (3) FeO to Fe at 870 K were reported by many researchers [22,23]. The reported TPR profiles of the iron phosphate also showed three reduction peaks. The first peak was due to the formation of $\text{Fe}_3(\text{P}_2\text{O}_7)_2$ from FePO_4 . The second peak was ascribed to the formation of $\text{Fe}_2\text{P}_2\text{O}_7$. The third peak represented the reduction of Fe and P species, probably to the elemental state [24,25]. Iron phosphate was the main component on the calcined precursor of the $\text{FeP}_{1/2}/\text{SiO}_2$ sample. The reduction of this sample should be similar to that of iron phosphate. Therefore, the three peaks in the profile of the $\text{FeP}_{1/2}/\text{SiO}_2$ sample was attributed to the three reduction stages of iron phosphate. In the case of the $\text{FeP}_{1/4}/\text{SiO}_2$ and $\text{FeP}_{1/8}/\text{SiO}_2$ samples, iron oxide was the major component on the calcined precursors. The first peak of these two samples at ~660 K was the overlapped reduction from Fe_2O_3 to Fe_3O_4 and from FePO_4 to $\text{Fe}_3(\text{P}_2\text{O}_7)_2$. The peaks at 758 and 870 K corresponded to the reduction from Fe_3O_4 to FeO and FeO to Fe , respectively. The last peak represented the formation of phosphides. For precursors with lower P contents, the TPR profiles showed more shoulder peaks, giving a more complicated overall reduction pattern. In fact, the amount of P was not sufficient to form Fe_3P and Fe_2P crystal phases for all the Fe in the cases of the precursors with lower P con-

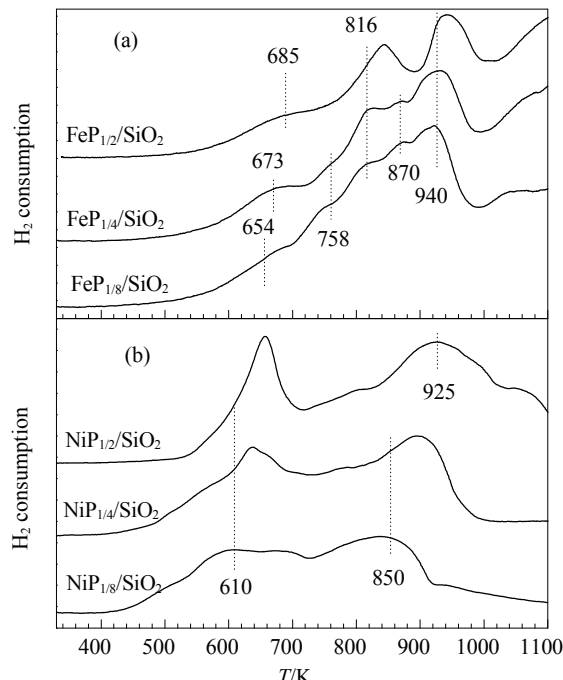


Fig. 1. TPR profiles of the calcined phosphate precursors of $\text{FeP}_x/\text{SiO}_2$ (a) and $\text{NiP}_x/\text{SiO}_2$ (b).

tents. Consequently, excess iron species would be transformed into metallic Fe before the reduction of phosphorus oxide, which would in turn assist the reduction of the other components by H₂ spillover [26,27]. The final peak at about 940 K shifted a little towards lower temperatures as the P loading decreased. This suggested that the assisting effect of reduced metallic Fe on the reduction of phosphorus species was weak.

The H₂-TPR profiles of the NiP_x/SiO₂ catalyst precursors are shown in Fig. 1(b). The first peak at 610 K was ascribed to the reduction of nickel species. The higher temperature peak at 850–925 K was ascribed to the reduction of the P–O bond [17,28,29]. This may be caused by the formation of phosphides species. It can be observed from Fig. 1(b) that the reduction of the P–O bond in the precursors became easier with the decrease of the P content because its peak temperature on the NiP_{1/8}/SiO₂ catalyst was decreased by 75 K compared with that of the NiP_{1/2}/SiO₂ catalyst. This was attributed to the effect of the active atomic hydrogen species from the dissociation of H₂ on metallic Ni formed earlier during the reduction [26,27]. This indicated that the interaction between the Ni and phosphorus species was stronger than those of the Fe samples. During the TPR, the mass spectrometer did not detect any PH₃ signal.

2.2 XRD characterization

The diffraction patterns of the fresh and spent FeP_x/SiO₂ catalysts are presented in Fig. 2(a). In the case of the FeP_{1/2}/SiO₂ sample, an almost pure Fe₂P phase was obtained in the fresh catalyst. There was a small amount of the Fe₃P phase, which may be from a small loss of P during calcination. No obvious difference was observed between the pattern of the spent FeP_{1/2}/SiO₂ catalyst and the fresh one. This indicated that the Fe₂P and Fe₃P phases were stable under the syngas atmosphere. Three crystal phases of metallic Fe, Fe₂P, and Fe₃P were present in the fresh FeP_{1/4}/SiO₂ catalyst. It was interesting to find that most of the metallic Fe phase transformed into iron carbide (Fe₅C₂), which is the active phase in F-T synthesis [30,31], while the Fe₂P and Fe₃P phases remained intact after CO hydrogenation just as in the FeP_{1/2}/SiO₂ sample. It appeared that the transformation of the metallic Fe phase had no impact on the Fe₂P and Fe₃P phases. The changes in the XRD patterns between the fresh and the spent catalysts for FeP_{1/8}/SiO₂ were similar to those of the FeP_{1/4}/SiO₂ sample. The difference was that the metallic Fe peak in the fresh catalyst became more intense and the Fe₃P phase was the main phosphide component.

The diffraction patterns of the fresh and spent NiP_x/SiO₂ catalysts are presented in Fig. 2(b). In the patterns of the NiP_x/SiO₂ catalysts, the nickel phosphide phases became complicated because different nickel phosphide phases with

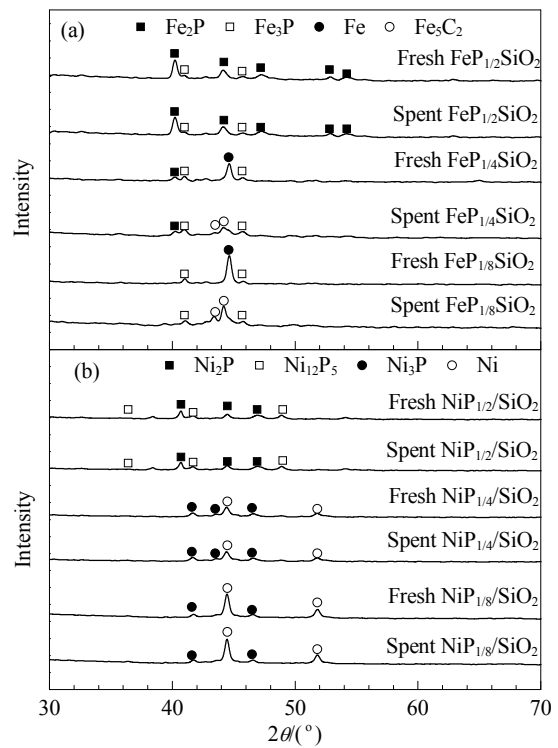


Fig. 2. XRD patterns of FeP_x/SiO₂ (a) and NiP_x/SiO₂ (b) catalysts before and after reaction.

different molar ratios of P to Ni were formed. In the case of the NiP_{1/2}/SiO₂ catalyst prepared from oxidic precursors with P:Ni = 1:2, the main phases on the fresh catalyst were Ni₂P and Ni₁₂P₅. The possible reason for this was that P was lost during calcination and reduction. This phenomenon of two nickel phosphide phases was also observed by Sawhil et al. [15] whose nickel phosphide was also prepared from a NiP_x/SiO₂ precursor with a molar ratio P:Ni = 1:2. The peak at 47° was a little broader because this peak is the result of the overlap of two peaks. One was a minor peak attributed to Ni₂P located at 47.4° and another was also a minor peak belonged to Ni₁₂P₅ at 46.9°. It was found that the metallic Ni phase appeared in the fresh catalyst, while the Ni₂P and Ni₁₂P₅ phases became the Ni₃P phase when the molar ratio of P to Ni was increased to 1:4 and 1:8. The XRD patterns of the spent nickel samples were unchanged from those of the corresponding fresh samples, which implied that the metallic Ni, Ni₂P, Ni₃P, and Ni₁₂P₅ phases were stable during the CO hydrogenation reaction. No other peaks associated with phosphorous species except for the phosphides appeared in the XRD patterns.

2.3 Textural properties and chemisorption of CO

N₂ adsorption was used to measure the surface area, pore diameter, and pore volume of the catalysts. CO chemisorp-

Table 1 Specific surface area and CO chemisorption over the fresh phosphide catalysts

Catalyst	Specific surface area (m^2/g)	Average pore diameter (nm)	CO uptake ($\mu\text{mol}/\text{g}_{\text{cat}}$)
SiO_2	180	19.9	0
$\text{FeP}_{1/2}/\text{SiO}_2$	120	19.4	15
$\text{FeP}_{1/4}/\text{SiO}_2$	124	19.0	24
$\text{FeP}_{1/8}/\text{SiO}_2$	133	18.7	75
$\text{NiP}_{1/2}/\text{SiO}_2$	134	18.8	10
$\text{NiP}_{1/4}/\text{SiO}_2$	147	17.5	30
$\text{NiP}_{1/8}/\text{SiO}_2$	149	16.9	46

tion capacities were also measured. The results are listed in Table 1. In comparison with the support, the fresh catalysts possessed lower specific areas and smaller average pore diameters, which was presumably due to pore blockage by the phosphides. The surface areas of the catalysts became smaller with increasing P content. CO uptake was small for pure fresh phosphide catalysts with a P:metal ratio of 1:2 in all cases. The enhanced CO uptake with the increase of the P:metal ratio can be attributed to adsorption on metallic active sites. The high calcination and reduction temperatures can induce a strong interaction between the support and the metal, which would weaken the CO adsorption capacity of the catalyst [32,33].

2.4 CO-TPD results

Figure 3(a) displays the TPD spectra of CO adsorbed on

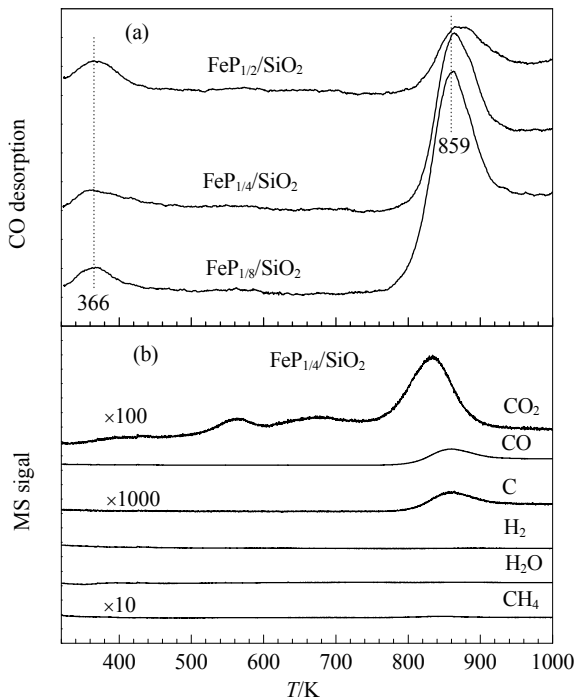


Fig. 3. CO-TPD profiles (a) and the mass spectra (b) during the CO-TPD on $\text{FeP}_x/\text{SiO}_2$ catalysts.

the $\text{FeP}_x/\text{SiO}_2$ catalysts. CO-TPD is a powerful tool to show the strength of the CO-metal bond, and the peak position of CO desorption is related to the kind of active site. The mass spectrum of the corresponding products during the CO-TPD over the $\text{FeP}_{1/4}/\text{SiO}_2$ catalyst is also shown in Fig. 3(b). In Fig. 3(a), two desorption peaks can be observed. The peak at the low temperature of 366 K was due to weakly adsorbed CO. The other peak at 859 K was attributed to strongly adsorbed CO on reduced metal particles. Figure 3(b) showed that the signals of CO_2 and C were detected during CO desorption at high temperature. This showed that the reaction of CO disproportionation ($2\text{CO} \rightarrow \text{CO}_2 + \text{C}$) took place during CO-TPD at 859 K. With the decrease of P to Fe molar ratio, the low and high desorption peak temperatures did not shift, and only the peak area of the high temperature peak increased. This suggested that the formation of phosphides induced the CO adsorption capacity decrease at the high temperature. XRD analysis showed that the metallic Fe was transformed into iron carbide during the reaction. Therefore, the CO-TPD profiles over the fresh catalysts may only partially reflect the interaction between adsorbed CO and active sites.

Figure 4(a) displays the TPD spectra of CO adsorbed on the $\text{NiP}_x/\text{SiO}_2$ catalysts. The mass spectrum of the corresponding products during CO-TPD over the $\text{NiP}_{1/4}/\text{SiO}_2$ catalyst is also shown in Fig. 4(b).

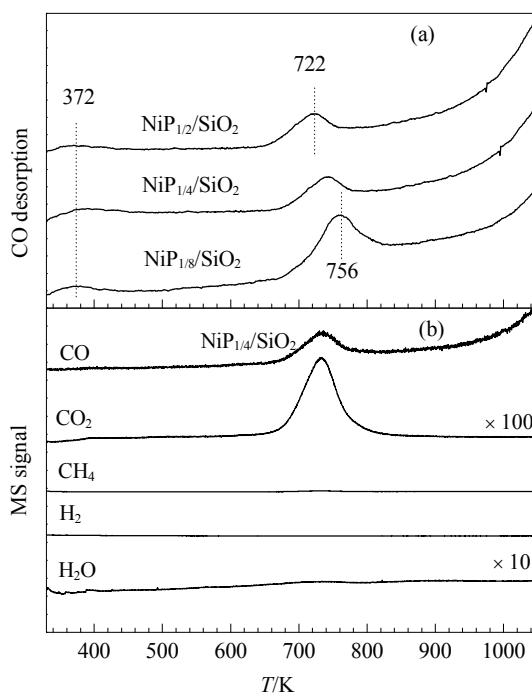


Fig. 4. CO-TPD profiles of $\text{NiP}_x/\text{SiO}_2$ catalysts (a) and mass spectra of $\text{NiP}_{1/4}/\text{SiO}_2$ during CO-TPD (b).

The desorption profiles of the $\text{NiP}_x/\text{SiO}_2$ catalysts were similar to those of the $\text{FeP}_x/\text{SiO}_2$ catalysts. The peak at 372

K was due to weakly adsorbed CO, and the peak at 722 K corresponded to strongly adsorbed CO. Judging from the simultaneous appearance of CO₂ during CO desorption at about 736 K in mass spectrum of the NiP_{1/4}/SiO₂ catalyst, the reaction of CO disproportionation also took place. With the decrease of the P:Ni molar ratio, the high temperature desorption peak was shifted noticeably from 722 to 756 K. This indicated that the introduction of P changed the electronic structure and weakened the adsorption of nickel. The weakening of the interaction between CO and nickel may enhance the selectivity for oxygenates in the product.

2.5 Catalytic performance

Table 2 presents the detailed reaction data from CO hydrogenation over the different phosphide catalysts. The supported pure iron metal catalyst produced mainly hydrocarbons. CO conversion and hydrocarbon selectivity increased with the decrease of the P:metal ratio, while the selectivity for oxygenates had an opposite trend. For the catalysts with the same ratio of metal to P, the CO conversion on the iron phosphide was a little higher than that on the nickel phosphides. The proportion of higher hydrocarbons in the product was also higher than that from the nickel phosphides. This was attributed to the phase transformation of metallic iron to iron carbide, which was shown by the XRD analysis. Iron carbide is very active for the synthesis of higher hydrocarbons from syngas [30,31], so a catalyst containing this phase would give some liquid phase with higher hydrocarbons. For the same ratio of metal to P, the low selectivity to higher hydrocarbons over the nickel phosphides indicated a limited chain growth ability of the nickel phosphide catalysts.

On decreasing the P:Fe ratio, the selectivity for methanol decreased rapidly from 30.1% to 10.6%, while those to methane and CO₂ increased slowly from 25.1% to

33.1% and from 7.8% to 15.3%, respectively. This was because the proportion of metallic iron in the catalysts increased with the decrease of the P:Fe ratio, resulting in the enhancement of the CO dissociation ability of the catalysts. It is known that Fe-based catalysts catalyze the water gas shift (WGS) reaction simultaneously during the CO hydrogenation reaction [30]. Our reaction results showed that pure iron phosphide also possessed WGS activity. It is worthwhile to note that the selectivity for oxygenates over Fe₂P reached as high as 50%, although the main product was methanol. This suggested that the Fe₂P phase was more conducive to the formation of oxygenates than metallic iron and iron carbide, although hydrocarbons were also produced on it. We have shown in the TPR characterization that the interaction between metallic Fe and reduced P was not very strong. Therefore, the coexistence of iron phosphide and metallic iron in the catalysts would give rise to two kinds of active sites that were mutually independent. The phosphide active site favored the formation of oxygenates and the active sites of metallic iron and iron carbide preferentially produced hydrocarbons. From the above observations, we deduced that CO hydrogenation over the FeP_{1/4}/SiO₂ and FeP_{1/8}/SiO₂ catalysts was an additive result of the actions of these two isolated active sites.

On decreasing the P:Ni ratio, the selectivity for methane increased slowly, while the selectivity for methanol showed a small decrease. The main component in the liquid product over the NiP_x/SiO₂ catalyst was methanol, which is similar to that of Cu based catalysts [5]. The selectivity for C₂⁺ oxygenates on this catalyst was relatively low. This was reasonable because metallic Ni possessed only very weak chain growth ability, and it is well known that Ni-based catalysts are good methanation catalysts [34]. The introduction of phosphorus changed the electronic properties of the metallic Ni particles. Thus, CO dissociation ability decreased, which was accompanied by an increase in the non-

Table 2 CO hydrogenation over the FeP_x/SiO₂ and NiP_x/SiO₂ catalysts

Catalyst ^a	CO conversion (%)	Selectivity (%)						
		CH ₄	C _{2~5} H ^b	C ₅₊ H ^c	MeOH	EtOH	Other C ₂₊ oxy ^d	CO ₂
FeP _{1/2} /SiO ₂	2.0	25.1	12.5	2.0	30.1	7.4	15.1	7.8
FeP _{1/4} /SiO ₂	6.5	29.4	15.4	5.0	19.4	9.9	10.2	10.7
FeP _{1/8} /SiO ₂	11.5	33.1	15.4	10.1	10.6	9.8	5.7	15.3
Fe/SiO ₂	19.2	32.4	22.6	20.2	2.7	2.0	2.0	18.1
NiP _{1/2} /SiO ₂	1.3	27.1	12.6	0	45.4	6.7	3.1	5.1
NiP _{1/4} /SiO ₂	2.5	38.5	8.6	0	44.4	4.3	1.2	3.0
NiP _{1/8} /SiO ₂	4.6	40.4	7.3	0	42.8	4.2	1.3	4.0
Ni/SiO ₂	14.5	80.2	5.2	0	2.2	0.9	0.0	11.5

Reaction conditions: $T = 553\text{ K}$, $p = 5.0\text{ MPa}$, H₂:CO = 2:1, GHSV = 5000 h⁻¹.

^aMetal loading of all catalysts was 10 wt%, and phosphorus loadings were different.

^bHydrocarbons with two to five carbons.

^cHydrocarbons with more than five carbons.

^dOxygenates other than ethanol with two to five carbons, such as propanal, propanol, butanol, butyraldehyde, and ethyl acetate.

dissociative CO adsorption capacity. Therefore, a large amount of liquid products, with methanol as the main component, was formed during CO hydrogenation over the $\text{NiP}_x/\text{SiO}_2$ catalysts.

3 Conclusions

CO hydrogenation over a series of iron group metal phosphide catalysts was investigated and correlated with the ratio of P to metal. The $\text{FeP}_x/\text{SiO}_2$ catalysts gave mixed oxygenates with methanol as the main component. The $\text{NiP}_x/\text{SiO}_2$ catalysts gave mainly methanol. The Fe_2P , Fe_3P , Ni, Ni_2P , Ni_3P , and Ni_{12}P_5 phases were stable during CO hydrogenation, while most of the metallic Fe phase was transformed into iron carbide. CO hydrogenation over the $\text{FeP}_x/\text{SiO}_2$ catalysts was an additive result from the two isolated active sites of iron phosphide and iron carbide. The influence of P caused the CO dissociation ability of nickel to decrease, which was accompanied by an increase in the nondissociative CO adsorption capacity.

References

- Subramani V, Gangwal S K. *Energy Fuels*, 2008, **22**: 814
- Burch R, Hayes M J. *J Catal*, 1997, **165**: 249
- Yin H M, Ding Y J, Luo H Y, Yan L, Wang T, Lin L W. *Energy Fuels*, 2003, **17**: 1401
- Haider M A, Gogate M R, Davis R J. *J Catal*, 2009, **261**: 9
- Tien-Thao N, Zahedi-Niaki M H, Alamdar H, Kaliaguine S. *Appl Catal A*, 2007, **326**: 152
- Chu W, Kieffer R, Kienemann A, Hindermann J P. *Appl Catal A*, 1995, **121**: 95
- Tien-Thao N, Zahedi-Niaki M H, Alamdar H, Kaliaguine S. *J Catal*, 2007, **245**: 348
- Jiao G, Ding Y, Zhu H, Li X, Li J, Lin R, Dong W, Gong L, Pei Y, Lu Y. *Appl Catal A*, 2009, **364**: 137
- Fang Y Z, Liu Y, Zhang L H. *Appl Catal A*, 2011, **397**: 183
- Wu X M, Guo Y Y, Zhou J M, Lin G D, Dong X, Zhang H B. *Appl Catal A*, 2008, **340**: 87
- Zhao L H, Fang K G, Jiang D, Li D B, Sun Y H. *Catal Today*, 2010, **158**: 490
- Surisetty V R, Dalai A K, Kozinski J. *Appl Catal A*, 2010, **381**: 282
- Oyama S T. *J Catal*, 2003, **216**: 343
- Zuzaniuk V, Prins R. *J Catal*, 2003, **219**: 85
- Sawhill S J, Layman K A, Vanwyk D R, Engelhard M H, Wang C M, Bussell M E. *J Catal*, 2005, **231**: 300
- Burns A W, Gaudette A F, Bussell M E. *J Catal*, 2008, **260**: 262
- Li K, Wang R, Chen J X. *Energy Fuels*, 2011, **25**: 854
- 黄金花, 陈吉祥. 催化学报 (Huang J H, Chen J X). *Chin J Catal*, 2012, **33**: 790
- Zaman S, Smith K. *Catal Commun*, 2009, **10**: 468
- Zaman S F, Smith K J. *Appl Catal A*, 2010, **378**: 59
- Zaman S F, Smith K J. *Catal Today*, 2011, **171**: 266
- Hayashi H, Chen L Z, Tago T, Kishida M, Wakabayashi K. *Appl Catal A*, 2002, **231**: 81
- Zhang H J, Ma H F, Zhang H T, Ying W Y, Fang D Y. *Catal Lett*, 2012, **142**: 131
- Nagaraju P, Srilakshmi C, Pasha N, Lingaiah N, Suryanarayana I, Prasad P S S. *Appl Catal A*, 2008, **334**: 10
- Nagaraju P, Lingaiah N, Balaraju A, Prasad P S S. *Appl Catal A*, 2008, **339**: 99
- Oyama S T, Wang X, Lee Y K, Bando K, Requejo F G. *J Catal*, 2002, **210**: 207
- Rodriguez J A, Hanson J C, Frenkel A I, Kim J Y, Perez M. *J Am Chem Soc*, 2002, **124**: 346
- Liu X G, Chen J X, Zhang J Y. *Catal Commun*, 2007, **8**: 1905
- Chen J X, Chen Y, Yang Q, Li K L, Yao C C. *Catal Commun*, 2010, **11**: 571
- OBrien R J, Xu L G, Spicer R L, Davis B H. *Energy Fuels*, 1996, **10**: 921
- Cheng J, Hu P, Ellis P, French S, Kelly G, Lok C M. *J Phys Chem C*, 2010, **114**: 1085
- Ojeda M, Rojas S, Garcia-Garcia F J, Granados M L, Terreros P, Fierro J L G. *Catal Commun*, 2004, **5**: 703
- Jablonski J M, Potoczna-Petru D, Okal J, Krajczyk L. *React Kinet Catal Lett*, 1995, **54**: 15
- Schoubye P. *J Catal*, 1969, **14**: 238